

Article

Time-Dependent Shrinkage Model for Recycled Fine Aggregate Thermal Insulation Concrete

Xuhang Zang, Pinghua Zhu *, Chunhong Chen, Xiancui Yan and Xinjie Wang

Changzhou City Key Laboratory of Building Energy-Saving Technology, Department of Civil Engineering, Changzhou University, Changzhou 213164, China; zangxuhangcczu@163.com (X.Z.); chench@cczu.edu.cn (C.C.); hhuyanxc@163.com (X.Y.); wangxinjie@cczu.edu.cn (X.W.)

* Correspondence: zph@cczu.edu.cn

Abstract: In this study, the shrinkage performance of recycled aggregate thermal insulation concrete (RATIC) with added glazed hollow beads (GHB) was investigated and a time-dependent shrinkage model was proposed. Two types of recycled fine aggregate (RFA) were used to replace natural fine aggregate in RATIC: RFA from waste concrete (RFA1) and waste clay brick (RFA2). Besides, the mechanical properties and thermal insulation performance of RATIC were also studied. Results showed that the pozzolanic reaction caused by RFA2 effectively improved the mechanical properties of RATIC; 75% was the optimal replacement ratio of RATIC prepared by RFA2. Added RFA decreased the thermal conductivity of thermal insulation concrete (TIC). The total shrinkage strain of RATIC increased with the increase of the replacement ratio of RFA. The 150d total shrinkage of RATIC prepared by RFA1 was 1.46 times that of TIC and the 150d total shrinkage of RATIC prepared by RFA2 was 1.23 times. The addition of GHBs led to the increase of early total shrinkage strain of concrete. Under the combined action of the higher elastic modulus of RFA2 and the pozzolanic components contained in RFA2, the total shrinkage strain of RATIC prepared by RFA2 with the same replacement ratio was smaller than that of RATIC prepared by RFA1. For example, the final total shrinkage strain of RATIC prepared by RFA2 at 100% replacement ratio was about 18.6% less than that of RATIC prepared by RFA1. A time-dependent shrinkage model considering the influence of the elastic modulus of RFA and the addition of GHB on the total shrinkage of RATIC was proposed and validated by the experimental results.

Keywords: glazed hollow bead; recycled fine aggregate; recycled fine aggregate thermal insulation concrete; time-dependent shrinkage model; shrinkage development



Citation: Zang, X.; Zhu, P.; Chen, C.; Yan, X.; Wang, X. Time-Dependent Shrinkage Model for Recycled Fine Aggregate Thermal Insulation Concrete. *Materials* **2021**, *14*, 5581. <https://doi.org/10.3390/ma14195581>

Academic Editor: Zhengwu Jiang

Received: 3 September 2021

Accepted: 22 September 2021

Published: 26 September 2021

Publisher's Note: MDPI stays neutral with regard to jurisdictional claims in published maps and institutional affiliations.



Copyright: © 2021 by the authors. Licensee MDPI, Basel, Switzerland. This article is an open access article distributed under the terms and conditions of the Creative Commons Attribution (CC BY) license (<https://creativecommons.org/licenses/by/4.0/>).

1. Introduction

With the development of concrete construction, a large number of old buildings with brick and concrete structures will be demolished. Recycled coarse aggregate (RCA) and recycled fine aggregate (RFA) are the main products after the demolition of brick and concrete structures [1]. For the RFA, recycled fine aggregate of waste concrete (RFA1) and recycled fine aggregate of waste clay brick (RFA2) are two common types [2]. Recycling RFA can effectively solve the shortage of natural river sand resources. Recently, the mechanical properties and durability of concrete containing RFA1 and RFA2 have been studied. Wang et al. [3] found that the compressive strength of recycled fine aggregate concrete (RFAC) containing RFA1 at 28 days was greater than the ordinary concrete. Kirthika et al. [4] systematically studied the durability of RFAC with RFA1 and results showed that concrete with 30% RFA1 had better resistance to chloride penetration and carbonation. Dang et al. [5] found that the compressive strength of RFAC containing 50% RFA2 with no extra water was comparable with ordinary concrete. It is a significant issue to study the performance of RFAC for the utilization of RFA.

Recycled aggregate thermal insulation concrete (RATIC) is a new type of green structural concrete, with the glazed hollow beads (GHB) and recycled aggregate [6,7]. It not

only alleviates environmental problems caused by construction and demolition waste but also reduces the overall energy consumption of buildings [8]. At present, research mainly focuses on the mechanical properties and thermal conductivity of RATIC. Wang et al. [9] carried out a systematic study on the mechanical properties of RATIC prepared with RCA, and the results showed that the compressive strength, splitting tensile strength and elastic modulus of RATIC were all lower than those of the GHB thermal insulation concrete (TIC). Xiao et al. [10] found that the thermal conductivity of recycled concrete decreased with the increase of the replacement ratio of RCA. The test results of Zhao et al. [11] showed that the thermal conductivity of concrete decreased significantly with the increase of GHB content. Nevertheless, few reports related to the performance of RATIC containing RFA.

As a new green structural concrete, the shrinkage of concrete causes micro-cracks [12] and plays an important role in the design of the service limit state of structural members [13]. According to EN1992 [14], the total shrinkage of concrete is composed of two parts: autogenous shrinkage and drying shrinkage of concrete. Autogenous shrinkage of concrete is defined as the volume reduction that occurs without moisture exchange between the internal concrete and external environment [15]. Delsaute et al. [16] found that RFA1 was beneficial to reducing the autogenous shrinkage of concrete, which attributed to the combined effect of additional water and elastic modulus of RFA1. Zhang et al. [17] found there was a rapid increase in the autogenous shrinkage of RFAC during the first 60 days, and then the increasing rate reduced. Moreover, Zhang et al. [18] find that the autogenous shrinkage strain of RFAC prepared by RFA2 decreased with the increase of the RFA2 replacements. Drying shrinkage is the volume reduction of hardened concrete caused by evaporation of water under the effect of unsaturated environmental humidity [19]. Khatib et al. [20] made a comparative study on the drying shrinkage of RFAC prepared by RFA1 and RFA2, and the 90-day drying shrinkage of RFAC prepared by RFA2 was significantly smaller than that prepared by RFA1. Zhang et al. [21] selected two different types of RFA1 and found that the water absorption and elastic modulus of RFA1 were the main reasons for the large difference in the final drying shrinkage strain of RFAC; based on the results, Zhang et al. [21] introduced the correction coefficients k_{wa} and k_v to modify the drying shrinkage model of ordinary concrete in EN1992 [14], which considered the influence of water absorption on the drying shrinkage development and the influence of elastic modulus on the final drying shrinkage strain of RFA1, respectively. Dang et al. [1] attributed the increase of drying shrinkage of RFAC prepared by RFA2 to the low elastic modulus of RFA2. Although many researches on the shrinkage of RFAC have been conducted, little information on the shrinkage of RATIC can be found in the literature.

At present, it is not common to conduct long-term shrinkage test as a routine test for every single concrete mixture, the structural engineer can only assess the risk of concrete cracking using existing prediction models [22]. In order to better represent the shrinkage of concrete in precast components, a large number of autogenous shrinkage, drying shrinkage and total shrinkage models have been established [23]. Maghfouri et al. [22] used five existing concrete shrinkage models to compare the shrinkage strain behavior of light weight concrete containing coarse aggregate and found that the EC2 model was the best prediction model to simulate the early shrinkage of light weight aggregate concrete. Bunderen et al. [24] compared the error between the total shrinkage model and the drying shrinkage model of concrete, and found that EC2 model could also be used to predict the drying shrinkage of concrete. Lai [25] et al. considered the influence of cementitious paste volume and wet packing density on the total shrinkage of concrete, and reduced the root mean square error of total shrinkage by optimizing the drying shrinkage in the AS3600 shrinkage equation. However, the prediction model of total shrinkage of RATIC containing GHB cannot be found in the literature.

In the present study, the shrinkage performance of RATIC containing GHB was investigated. Considering the influence of RFA and GHB, a time-dependent shrinkage model was proposed to predict the total shrinkage of RATIC. Besides, the mechanical

properties, thermal insulation performance and the scanning electron microscope (SEM) of RATIC were also studied.

2. Materials and Methods

2.1. Cementing Material

P•O 42.5 cement and fly ash were used as cementitious materials. The chemical components of cementitious materials listed in Table 1 met the requirements of Chinese standard GB/T 175-2007 [26].

Table 1. Chemical compositions of cementitious materials (%) [27].

Composition	SiO ₂	Al ₂ O ₃	Fe ₂ O ₃	TiO ₂	CaO	MgO	K ₂ O	N ₂ O
Cement	12.54	4.41	3.41	0.59	72.97	0.21	0.90	0.26
Fly ash	38.23	24.76	11.91	1.97	14.85	1.03	1.98	0.61

2.2. Aggregates

GHBs, produced by Jiangsu Huajia Building Materials Technology Co., Ltd, Zhenjiang, China, was added to concrete as a fine aggregate. The physical properties of GHBs are listed in Table 2. Figure 1a shows the GHBs after soaking in water for three months. The higher flotation ratio of GHBs in Figure 1a indicated that it was difficult for water to enter the inner cavity of GHB, and the absorbed water of GHBs was mainly attached to the surface or stored in the open pores. Figure 1b is the SEM image of GHB, open pores can be seen on the surface of GHB. Figure 1c is the sieve size distribution of GHB.

Table 2. Physical properties of GHB.

Size (mm)	Water Absorption (%)	Bulk Density (kg/m ³)	Thermal Conductivity (W/(m·K))	Cylinder Compressive Strength (kPa)
0.5–1.5	23	130	0.028	209

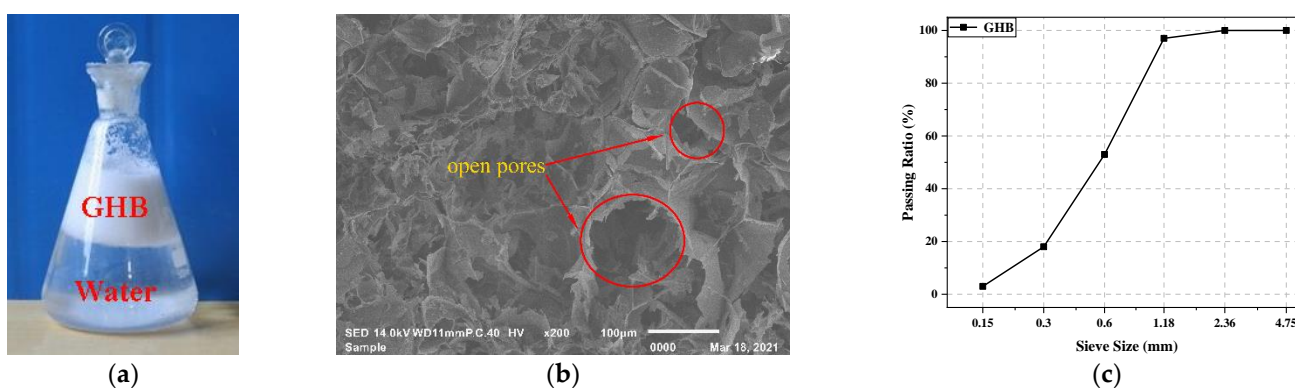


Figure 1. (a) The GHBs after soaking in water for three months and (b) SEM image of GHB and (c) Sieve size distribution of GHB.

Gravel and river sand was used as natural coarse aggregate (NCA) and NFA, respectively. Two different types of RFA were also used. RFA1 was prepared from waste concrete and RFA2 was prepared from waste clay bricks. The physical properties of aggregates were tested according to the Chinese standard GB/T 14684–2011 [28] and GB/T 14685–2011 [29], as shown in Table 3. Among them, the water absorption, moisture content and crushing value of RFA1 were higher than that of RFA2, and the apparent density was lower than that of RFA2. Overall, the physical properties of RFA1 were worse than that of RFA2.

Table 3. Physical properties of natural and recycled aggregate.

Aggregates	Apparent Density (kg/m ³)	Water Absorption (%)	Moisture Content (%)	Crushing Value (%)	Fineness Modulus
NFA	2650	0.3	0.03	13.20	2.4
RFA1	2330	9.53	4.84	21.88	2.4
RFA2	2350	6.39	1.53	18.41	2.4
NCA	2680	1.30	0.1	14.3	—

The particle size of coarse aggregate was 5–20 mm. In order to increase the performance comparability of different types of concrete, all gradations of fine aggregates were adjusted to make RFA1 and RFA2 gradations as consistent as possible with NFA gradations. The particle size distribution of the three kinds of fine aggregate is shown in Figure 2a, and their fineness modulus was all 2.4. The volumetric flask method was used to test the 24-h water absorption rate of RFA [30]. Figure 2b shows the variation of water content with time in RFA, and Figure 2c shows the variation trend after normalization treatment [31], that is the calculated value of $\omega(t)/\omega(t_{24h})$. As can be seen from Figure 2c, the water absorption rate of RFA1 was faster than that of RFA2.

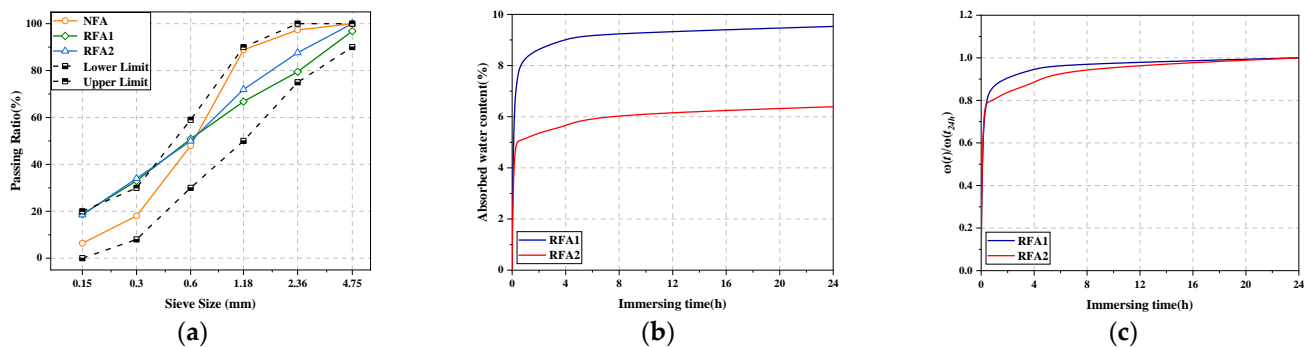


Figure 2. (a) Sieve size distribution of fine aggregates and (b) the variation of water content with time in RFA and (c) the variation trend of RFA water absorption after normalization treatment.

Figure 3a–c is the SEM images of NFA, RFA1 and RFA2, respectively. The surface of NFA was smooth and flat (Figure 3a), while there were obvious pores on the surface of RFA1 (Figure 3b). In addition, many small particles occurred on the surface of RFA1, namely old mortar particles in waste concrete. There were distinct lines on the surface of RFA2 (Figure 3c), which should be the sintered phase produced in the sintering process of clay bricks. RFA2 had a compact surface and clear structure with only a few micro pores. Comparing Figure 3b,c shows that the surface of RFA2 was denser than that of RFA1, indicating a better quality of RFA2.

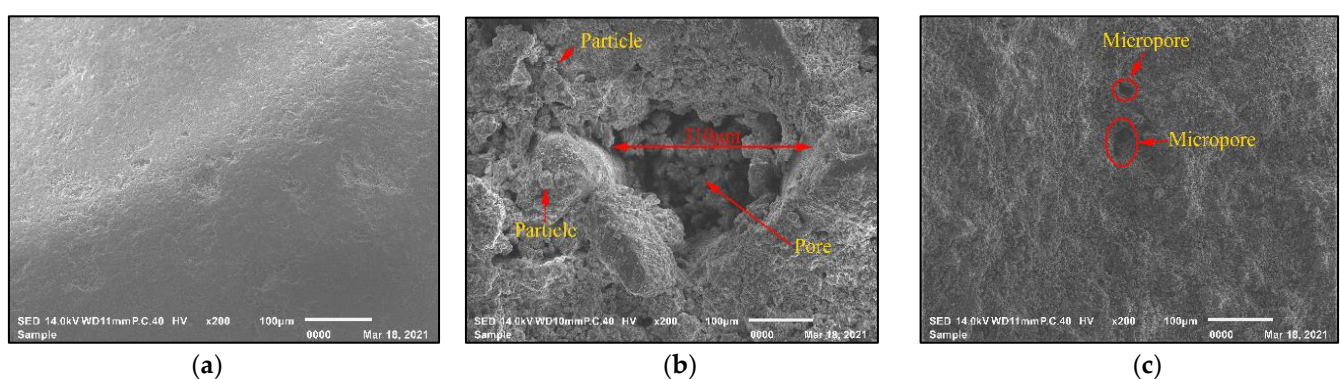


Figure 3. SEM images of (a) NFA, (b) RFA1 and (c) RFA2.

The chemical composition and main oxides of fine aggregate were analyzed by X-ray powder diffractometer (Rigaku, Japan) and X-ray fluorescence spectrometer (Bruker, Germany), respectively. The main oxides in fine aggregate are listed in Table 4. The chemical composition of fine aggregate is shown in Figure 4. It can be seen from Table 4 that the main chemical composition of NFA was SiO_2 , while the chemical composition of RFA1 and RFA2 were more complex. The content of CaO in RFA1 was as high as 27.91%. It can be seen from the XRD of RFA1 in Figure 4 that the main existing forms of CaO in RFA were CaCO_3 and Ca(OH)_2 . Compared with RFA1, the contents of Al_2O_3 and Fe_2O_3 in RFA2 were 6.35% and 3.74% higher, respectively. The total content of SiO_2 , Al_2O_3 and Fe_2O_3 in RFA2 was more than 70%, which met the requirement of the content of main chemical components of pozzolanic materials in ASTM C618 [32]. Therefore, RFA2 with sieve size less than 0.15 mm could be considered as a potential pozzolanic material [33].

Table 4. Chemical composition of recycled fine aggregate (%).

	SiO_2	CaO	Al_2O_3	Fe_2O_3	MgO	K_2O	SO_3	Na_2O	TiO_2	BaO	Cl
NFA	96.0	0.50	1.8	0.5	0.1	0.7	0.05	0.20	0.10	0.00	0.00
RFA1	50.52	27.91	11.88	2.09	2.13	1.77	1.33	0.77	0.74	0.26	0.18
RFA2	67.56	1.67	18.23	5.83	1.53	2.22	0.14	1.41	0.94	0.08	0.02

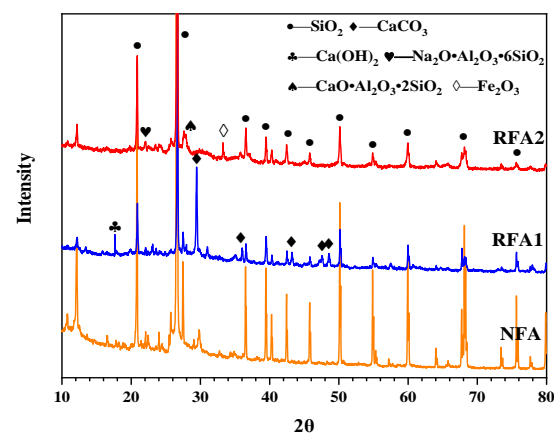


Figure 4. X-ray diffraction diagrams of fine aggregate.

2.3. Mix Proportions

In this study, RFA1 and RFA2 were used to replace NFA with different replacement ratios (25%, 50%, 75% and 100%) to prepare recycled aggregate thermal insulation concrete, namely RATIC1 and RATIC2. Considering the influence of GHBs and RFAs on the shrinkage performance of concrete, a group of NAC and a group of TIC specimens were designed as the control groups. Mix proportions of different types of concrete are shown in Table 5. In order to improve the performance of RATIC [34,35], additional water was added in the stirring process, where the additional water consumption was obtained by multiplying the difference between the 24-h water absorption and the moisture content of RFA by the mass amount of RFA. The superplasticizer with solid content of 40% was used to improve the performance of concrete.

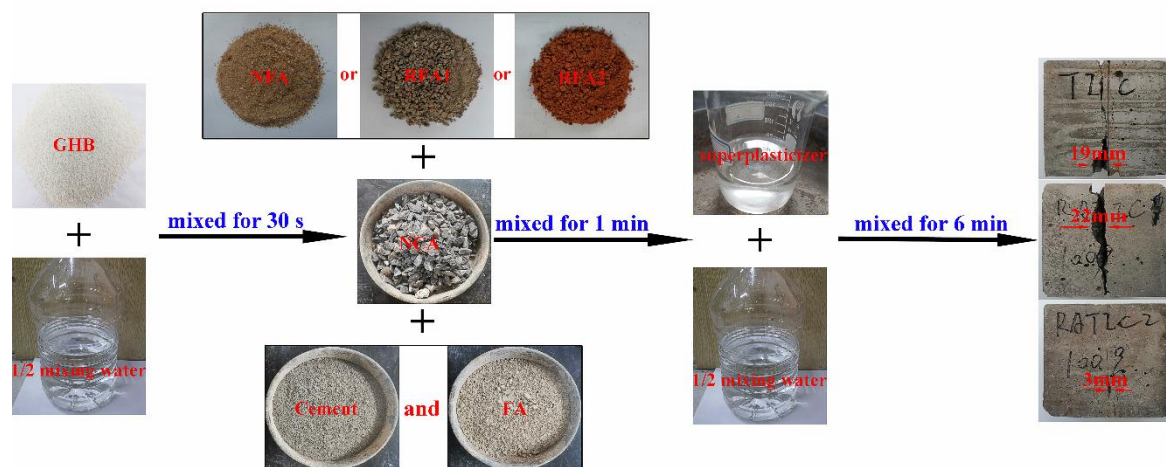
2.4. Specimen Preparation

The concrete mixing method referred to the method proposed by Wang et al. [6], as shown in Figure 5. For each type of concrete mixture, twenty-four 100 × 100 × 100 mm cubes, three 150 × 150 × 300 mm prisms, three 100 × 100 × 515 mm prisms and two φ200 × 400 mm cylinders were prepared.

Table 5. Mix proportions of RATIC under different replacement ratio (kg).

	Cement	FA ²	NFA	RFA	GHB	NCA	Water		SP ²	Slump (mm)
							MW ²	AW ²		
NAC	408	72	475	0	0	1110	240	—	0	180
TIC	408	72	475	0	130	1110	240	—	1.92	190
RATIC1-25 ¹	408	72	356	104	130	1110	240	4.88	2.88	185
RATIC1-50 ¹	408	72	238	209	130	1110	240	9.80	3.84	200
RATIC1-75 ¹	408	72	119	313	130	1110	240	14.68	4.80	205
RATIC1-100 ¹	408	72	0	418	130	1110	240	19.60	5.76	180
RATIC2-25 ¹	408	72	356	105	130	1110	240	5.10	2.88	195
RATIC2-50 ¹	408	72	238	211	130	1110	240	10.25	3.84	205
RATIC2-75 ¹	408	72	119	316	130	1110	240	15.36	4.80	210
RATIC2-100 ¹	408	72	0	421	130	1110	240	20.46	5.76	190

¹ For the nomenclature, taking 'RATIC1-100' as an example, RATIC1 stands for recycled aggregate thermal insulation concrete prepared with RFA1; 100 is the replacement ratio of RFA1. ² FA stands for fly ash; MW stands for mixing water; AW stands for additional water; SP stands for superplasticizer.

**Figure 5.** Schematic view of mixing procedures.

2.5. Test Methods

The slump of mixed concrete was measured according to GB/T 50080-2016 [36]. After casting, all specimens are maintained according to the Chinese standard [37]. The compressive strength of concrete at 3, 7, 14, 28, 60, 90, 150 days and the splitting tensile strength at 28 days were tested using the 100 × 100 × 100 mm cubes. The elastic modulus of concrete at 28 days was evaluated using the 150 × 150 × 300 mm prisms. The thermal conductivity of concrete at 28 days was evaluated using the $\phi 200 \times 400$ mm cylinders.

The shrinkage performance of concrete was tested according to GB/T 50082-2009 [38]. The shrinkage of concrete was measured using the 100 × 100 × 515 mm prisms. First, the specimen was put into standard curing room for 3 days; then, the specimen was immediately moved into a test chamber where the room temperature was maintained at $(20 \pm 2)^\circ\text{C}$ and the relative humidity was maintained at $(60 \pm 5)\%$. HSP-540 concrete shrinkage dilatometer (Blue standard building instrument Factory, Cangzhou, Heibei, China) was used to test the length of RATIC at different times, and the total shrinkage strain value of RATIC was obtained. The embedded probe was used in this test, and the size of the probe and HSP-540 concrete shrinkage dilatometer is shown in Figure 6. The initial calibration distance of the specimen was 470 mm, and the total shrinkage rate of concrete was measured over a period of 150 days.

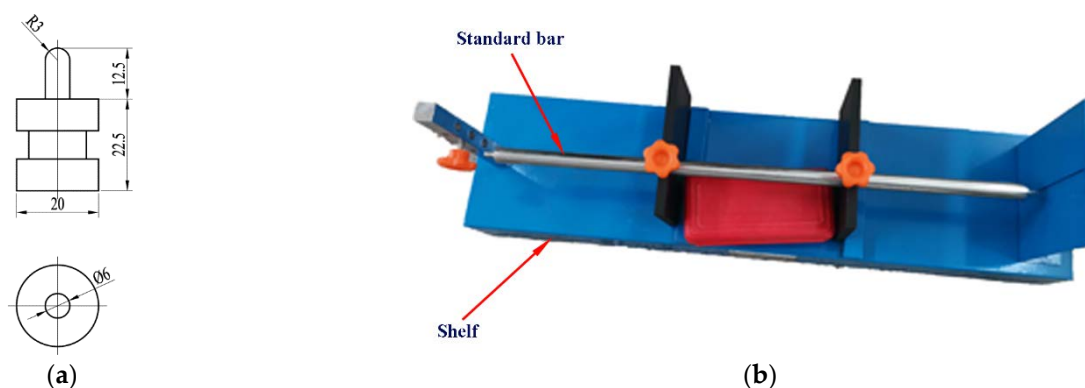


Figure 6. (a) Size of the probe and (b) HSP-540 concrete shrinkage dilatometer.

The microstructure of the ITZ of concrete between GHB and cement matrix, the ITZ of concrete between fine aggregate and cement matrix were observed by SEM. Before the experiment, the samples were soaked in ethanol for 24 h, and then dried in a vacuum-desiccant box at 60 °C for 24 h. The SEM images were captured by an JSM-IT100 equipment (JEOL, Japan) at 14 kV after the samples were spray-coated with gold.

3. Results and Discussion

3.1. Mechanical Properties of RATIC

3.1.1. Compressive Strength (f_c)

The compressive strength of RATIC at different ages is shown in Figure 7. Generally, the compressive strength of RATIC increased with the increasing ages. At the early ages, the difference between the compressive strength of NAC and TIC was narrow; adding GHB had no obvious effect on the compressive strength of TIC before 28 days. However, the compressive strength of NAC after 28 days was a little higher than that of TIC. At 150 days, the compressive strength of NAC was 8.5% higher than that of TIC.

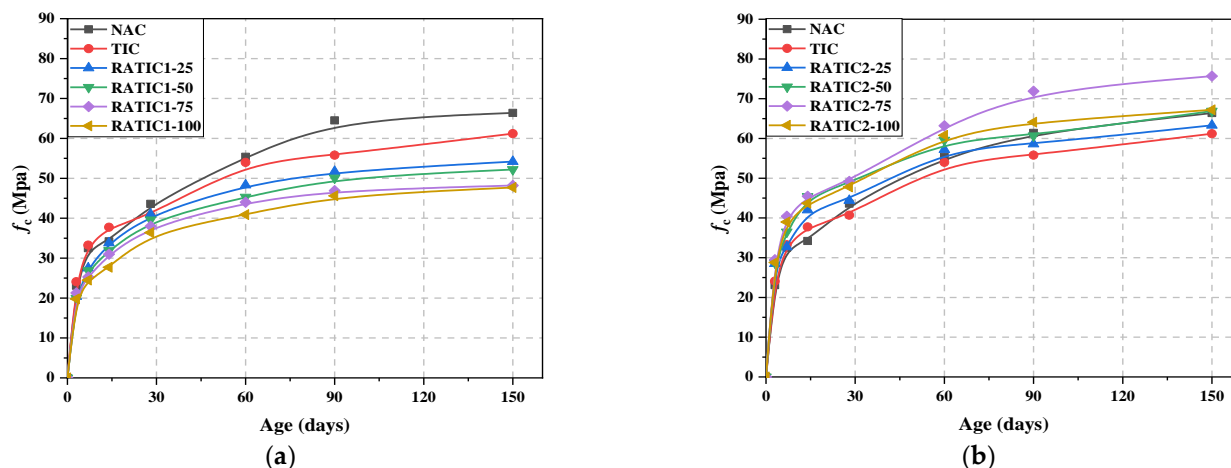


Figure 7. The compressive strength of RATIC at different ages: (a) RATIC1; (b) RATIC2.

As can be seen in Figure 7a, the compressive strength of RATIC1 decreased with the increase of replacement ratio of RFA1. For example, the compressive strength of RATIC containing 100% RFA1 at 150 days decreased by 22.1% compared to that of TIC containing no RFA1. However, in Figure 7b, the compressive strength of RATIC increased when RFA2 added. The maximum compressive strength of RATIC2 occurred in the RATIC2 specimen containing 75% RFA2. The compressive strength of RATIC2-75 at 150 days increased by 23.7% compared to that of TIC.

The chemical composition and physical properties of RFA1 and RFA2 were important factors affecting the compressive strength of RAT1C1 and RAT1C2. RFA1 had a higher water absorption and absorbed a large amount of water, which slowed down the hydration rate of cement. Besides, the crushing value of RFA1 was higher than that of RFA2. The poor physical and mechanical properties of RFA1 had a negative effect on the compressive strength of RAT1C. For the RAT1C2, the water absorption of RFA2 was smaller than that of RFA1. Adding RFA2 increased the compressive strength of RAT1C, which might be due to the reaction between $\text{Ca}(\text{OH})_2$ and pozzolanic material, producing new hydrated calcium silicate and providing additional strength for RAT1C2.

3.1.2. Splitting Tensile Strength (f_{spt})

The splitting tensile strength of RAT1C at 28 days is shown in Table 6. Generally, the splitting tensile strength increased first and decreased later with the increasing of RFA contents. For the RAT1C1, the maximum splitting tensile strength at 28 days occurred in the specimen containing 50% RFA1; for the RAT1C2, the maximum splitting tensile strength occurred in the specimen containing 75% RFA2. When the replacement ratio of RFA was relative low, the combination of the irregular surface of RFA and the penetration of the cement matrix to the surface of the RFA contributed to enhance the adhesion force of ITZ and improved the mechanical properties of RAT1C [5]. When the RFA contents increased, the larger crushing value of RFA could exert a bad effect on the mechanical properties of RAT1C. In addition, it was found that the splitting tensile strength of NAC at 28 days was slightly larger than that of TIC, which is in accordance with the results of compressive strength.

Table 6. Splitting tensile strength of RAT1C (MPa).

	NAC	TIC	RAT1C1				RAT1C2			
$r_{\text{RFA}} (\%)$			25	50	75	100	25	50	75	100
f_{spt}	3.73	3.44	3.73	3.81	3.58	2.99	4.51	4.72	4.81	4.25

3.1.3. Elastic Modulus (E_c)

The elastic modulus of RAT1C at 28 days is shown in Table 7. It can be seen that adding GHB greatly decreased the elastic modulus of RAT1C. The elastic modulus of TIC at 28 days was nearly 26.4% less than that of NAC, which could be owing to the porous property of lightweight aggregate of GHB. This phenomenon was similar with the results in [11] that adding GHB greatly reduced the elastic modulus of ordinary concrete. In addition, the variation of elastic modulus of RAT1C was similar with the splitting tensile strength; it increased first and decreased later with the increasing of RFA contents. The maximum elastic modulus of RAT1C1 and RAT1C2 occurred in specimen with 50% RFA1 and 75% RFA2, respectively. Besides, the elastic modulus of RAT1C2 were higher than that of RAT1C1. It can be seen from Table 3 that RFA2 has better physical properties, which was beneficial to the mechanical properties of RAT1C. Besides, the pozzolanic composition in RFA2 can also improve the elastic modulus of RAT1C2 [33].

Table 7. Elastic modulus of RAT1C (GPa).

	NAC	TIC	RAT1C1				RAT1C2			
$r_{\text{RFA}} (\%)$	0	0	25	50	75	100	25	50	75	100
E_c	31.4	23.1	23.4	26.7	22.6	15.1	23.8	28.2	30.8	25.9

3.2. Thermal Conductivity (K_c)

The thermal conductivity of RAT1C at 28 days is shown in Table 8. In Table 8, the thermal conductivity of NAC reduced nearly 40.1% when GHB added, indicating that

TIC had a better thermal insulation performance than NAC. In addition, the thermal conductivity of TIC could decrease when RFA added. For the RATI1, the minimum thermal conductivity occurred in specimen with 100% RFA1; for the RATI2, the minimum thermal conductivity occurred in specimen with 100% RFA2. This phenomenon might be attributed to the pores on the surface of the RFA that were not fully filled, which reduced the thermal conductivity of the RATI. Besides, irrespective of the RFA contents, the thermal conductivity of RATI1 was slightly smaller than that of RATI2, which could be due to the more and larger pores in RFA1.

Table 8. Thermal conductivity of RATI (W/(m·K)).

	NAC	TIC	RATIC1				RATIC2			
$r_{\text{RFA}}(\%)$	0	0	25	50	75	100	25	50	75	100
K_c	1.52	0.91	0.85	0.88	0.83	0.81	0.88	0.89	0.90	0.87

3.3. Total Shrinkage (ϵ_{cs})

The total shrinkage curve of concrete is shown in Figure 8. In Figure 8, the total shrinkage strain of TIC was greater than that of NAC. This may be because the addition of GHB reduced the overall elastic modulus of concrete aggregate and increased the air content of concrete. The decrease of the elastic modulus of the aggregate reflected the decrease of compressive strength of concrete to some extent. Therefore, it was no surprise that the final total shrinkage strain of TIC was larger than that of NAC.

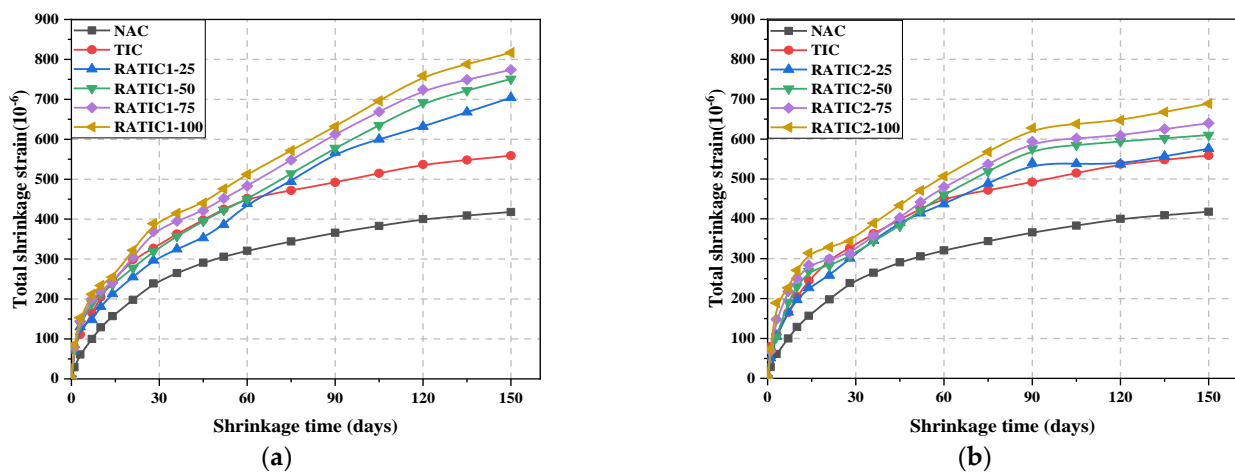


Figure 8. The total shrinkage curve of RATI with time: (a) RATI1; (b) RATI2.

In addition, the total shrinkage strain of RATI increased with the increase of RFA replacement ratio. The total shrinkage strain of RATI1-100 at 150 days was 1.46 times that of TIC, and the total shrinkage strain of RATI2-100 at 150 days was 1.23 times that of TIC. Besides, comparing Figure 8a,b shows that the total shrinkage strain of RATI1 was larger than RATI2, irrespective of the contents of RFA. This phenomenon could be due to the lower elastic modulus of RATI1; the lower elastic modulus of aggregate led to a higher shrinkage [21].

In order to compare the development of total shrinkage of RATI, the total shrinkage strain of NAC, TIC and RATI at different times was normalized to the final value, that is, $\epsilon_{cs}(t) / \epsilon_{cs}(t_{end})$, as shown in Figure 9a–c. As can be seen from Figure 9a, compared with NAC, the total shrinkage strain of TIC developed rapidly in the early stage, and the total shrinkage at 1 day and 3 days reached 14.31% and 19.86% of the total shrinkage, respectively, which were 106.3% and 36.1% higher than the corresponding total shrinkage of NAC. The main reason for this phenomenon may be the continuous progress of cement

hydration, which had a compaction effect on GHBs [39]; the volume deformation of GHBs occurred to a certain extent, which could increase the total shrinkage strain of RATIC at early stage. Maghfouri et al. [22] reached similar conclusions by adding oil palm shells to concrete. As also shown in Figure 9a, GHBs had little effect on the long-term development of total shrinkage strain of TIC, which may be due to the fact that the water adsorbed on the surface of GHBs and the water in the open pores dissipated quickly.

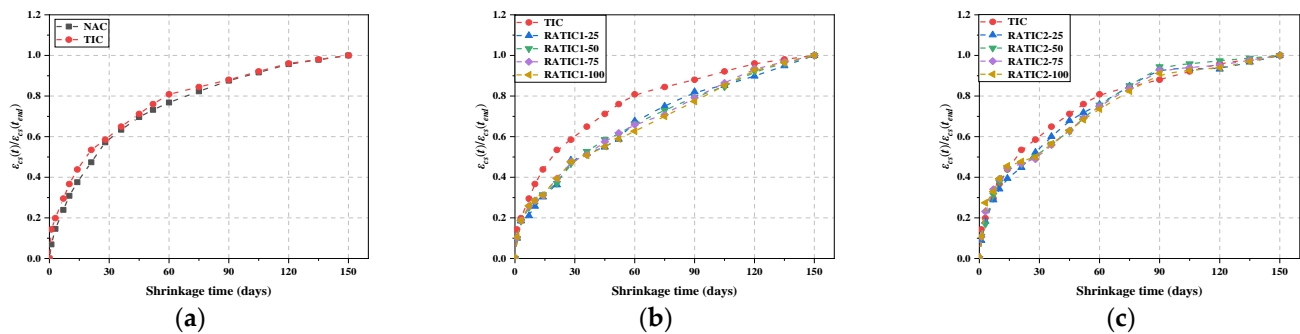


Figure 9. Normalized total shrinkage of (a) NAC and TIC, (b) RATIC1 and (c) RATIC2.

As can be seen from Figure 9b,c, the total shrinkage strains of RATIC1-100 at 3, 7 and 14 days were 18.7%, 25.9% and 31.2% of their 150 d total shrinkage strains, respectively. The total shrinkage strains of RATIC2-100 at 3, 7 and 14 days were 27.4%, 32.9% and 45.6% of their 150 d total shrinkage strains, respectively. In contrast to RATIC1, in the early stages of the total shrinkage development of RATIC2, the water was not only used for the cement hydration reaction, but also provided the water needed for the pozzolanic reaction in RFA2. Therefore, the internal environment of RATIC2 was drying faster than that of RATIC1 [40], which might be the main reason for the rapid development of total shrinkage strain in the early stage of RATIC2.

Moreover, as shown in Figure 9b, all curves of RATIC1 were significantly lower than TIC, which indicated a delay in the development of total shrinkage of RATIC1 when RFA1 added. This was due to the fact that the water stored in the RFA1 compensated for the water loss of the cement matrix and contributed significantly to the reduction in the drying shrinkage of the total shrinkage [21]. However, as shown in Figure 9c, RATIC2 did not show a significant delay in the development of total shrinkage. This may be because the long duration of the pozzolanic reaction consumed the water stored in RFA2, so the cement matrix of RATIC2 was unable to replenish water from RFA2.

3.4. SEM

Figure 10a shows the ITZ of TIC between GHB and the cement matrix. There was an obvious filling area between the cement matrix and GHB, and part of the cement matrix filled into the open pores of GHB. Cement matrix filling might be an important reason for the higher total shrinkage strain of TIC than that of NAC in the early stage. It is generally believed that the ITZ was the weak part of concrete, and the analysis of its microstructure was beneficial to further study the performance of concrete. In Figure 10b, there was an obvious ITZ in TIC between NFA and cement matrix. Figure 10c,d show the ITZ of RATIC1 and RATIC2 between fine aggregate and cement matrix, respectively. Compared with TIC in Figure 10b, the ITZ of RATIC1 (Figure 10c) and RATIC2 (Figure 10d) were denser, which explained that the splitting tensile strength and elastic modulus of RATIC1 and RATIC2 could be improved when the RFA replacement ratio was appropriate as shown in Tables 6 and 7. However, there were also old ITZs between the old natural aggregate and the old cement matrix in RFA1. As shown in Figure 10c, the old ITZ in RFA1 made the ITZ micromorphology more complex, and its length was larger than that of RATIC2, which resulted in worse mechanical properties of RATIC1.

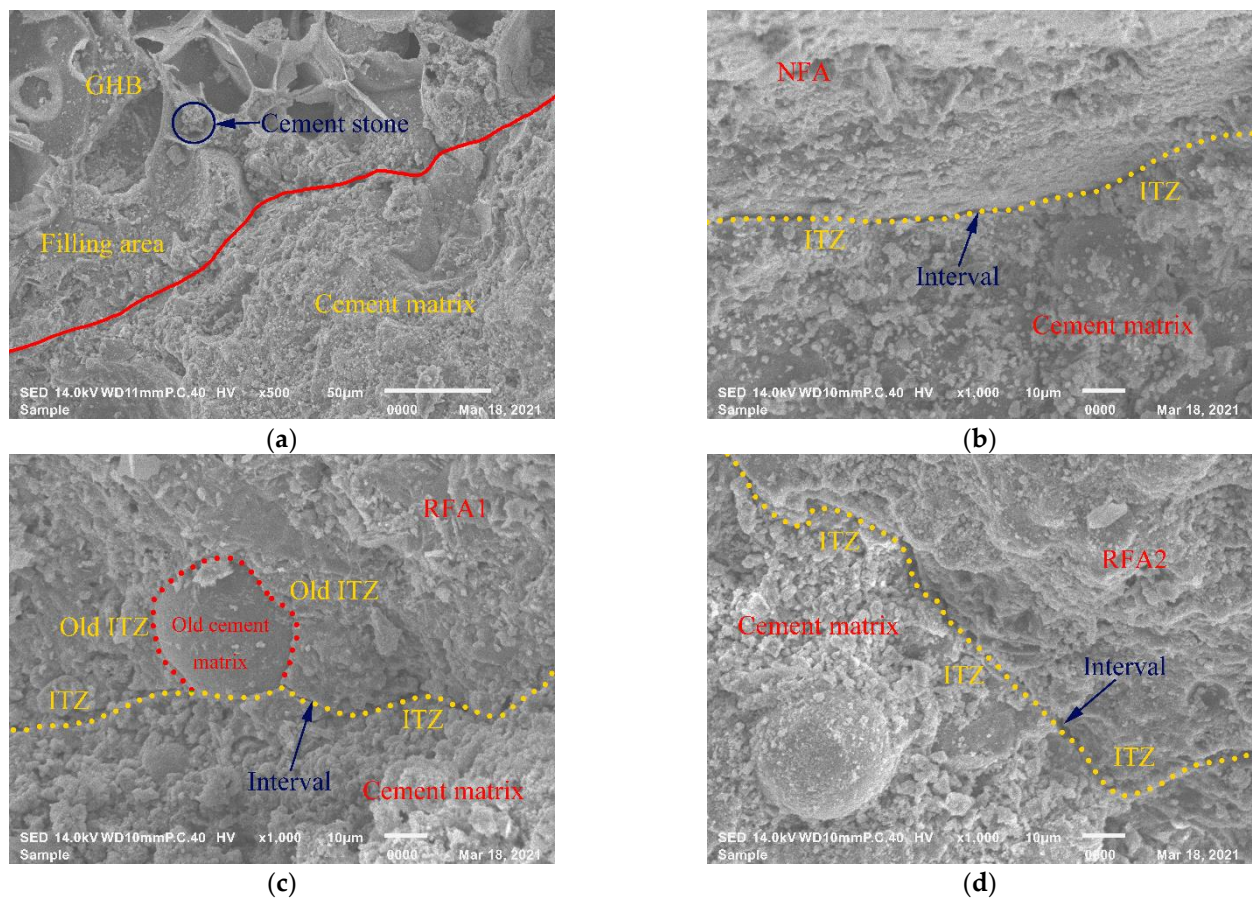


Figure 10. SEM images of (a) GHB in TIC (b) NFA in TIC, (c) RFA1 in RATIC1 and (d) RFA2 in RATIC2.

4. Time-Dependent Shrinkage Model

The total shrinkage strain ($\varepsilon_{cs,0}$) considered in the EC2 [41] prediction model is the sum of the autogenous shrinkage strain (ε_{ca}) and the drying shrinking strain (ε_{cd}). The specific calculation formulas of ε_{ca} and ε_{cd} are shown in Equations (1) and (2).

$$\varepsilon_{ca} = \left(1 - e^{-0.2t^{0.5}}\right) \varepsilon_{ca}(\infty) \quad (1)$$

$$\varepsilon_{cd} = \frac{(t - t_0)}{(t - t_0) + 0.04\sqrt{h_0^3}} k_h \varepsilon_{cd,0} \quad (2)$$

where t is the concrete age, in days; $\varepsilon_{ca}(\infty)$ is related to cylinder strength (f_{ck}) of concrete at 28 days; t_0 is the concrete age, in days, at the beginning of drying shrinkage; h_0 is the nominal thickness of concrete, and 2 times the ratio of the sectional area to the section circumference of the concrete member is taken; $\varepsilon_{cd,0}$ is the nominal unrestrained drying shrinkage values, which can be found in EN1992 [14]; k_h is the coefficient depending on the notional size h_0 .

The time-dependent shrinkage model for RATIC cites the time-dependent factor k_{wa} [21], considers the autogenous shrinkage strain amplification factor k_b and drying shrinkage strain amplification factor k_a of RATIC. The specific expression is shown in Equation (3):

$$\varepsilon_{cs} = \left(1 - e^{-0.2t^{0.5}}\right) k_b \varepsilon_{ca}(\infty) + \frac{(t - t_0)}{(t - t_0) + 0.04k_{wa}\sqrt{h_0^3}} \gamma_a k_a \varepsilon_{cd,0} \quad (3)$$

where k_b is the coefficient depending on the content of GHB; k_{wa} and k_a are the coefficients depending on water absorption and elastic modulus of RFA, respectively.

4.1. Shrinkage Model for TIC

In the process of concrete solidification and hardening, GHBs inevitably shrink in volume. Therefore, in Equation (5), an amplification factor k_b is introduced to ϵ_{ca} to modify the variation of shrinkage strain caused by the volume deformation of GHBs in TIC. By regression analysis of the experimental results of TIC, the autogenous shrinkage strain amplification factor k_b can be calculated. However, GHB is similar to the solid air-entraining agent, which increases the air content of TIC, thus increasing the ϵ_{cd} of TIC. According to the volume difference of concrete mixture [8], the volume fraction of GHB is about 25%, which can be considered as the air content intake of TIC and RATIC. The ACI-209-92 [41] model takes into account the influence of concrete air content on the total shrinkage strain of concrete, and gives the correction coefficient γ_α , whose specific value is shown in Equation (4):

$$\gamma_\alpha = 0.95 + 0.008\alpha \tag{4}$$

where γ_α is the air content factor, α is the air content expressed as a percentage.

The total shrinkage ($\epsilon_{cs,b}$) of TIC modified by the autogenous shrinkage strain amplification factor k_b and the air content correction factor γ_α is shown in Equation (5). The autogenous shrinkage strain amplification factor k_b in this experiment was 3.17 by regression analysis.

$$\epsilon_{cs,b} = \left(1 - e^{-0.2t^{0.5}}\right)k_b\epsilon_{ca}(\infty) + \frac{(t - t_0)}{(t - t_0) + 0.04\sqrt{h_0^3}}\gamma_\alpha\epsilon_{cd,0} \tag{5}$$

Figure 11a shows the prediction curve of NAC total shrinkage ϵ_{cs} based on the EC2 model, and Figure 11b is the prediction curve of TIC total shrinkage $\epsilon_{cs,b}$ optimized by the GHB influence factor k_b on the basis of the EC2 model. As shown in Figure 11, the EC2 model can well predict the change trend of the total shrinkage of NAC, but the predicted value of the total shrinkage of TIC differs greatly from the experimental results. However, the model shown in Equation (5) can well predict the variation trend of TIC total shrinkage, indicating that the modification of the EC2 model by introducing k_b is effective.

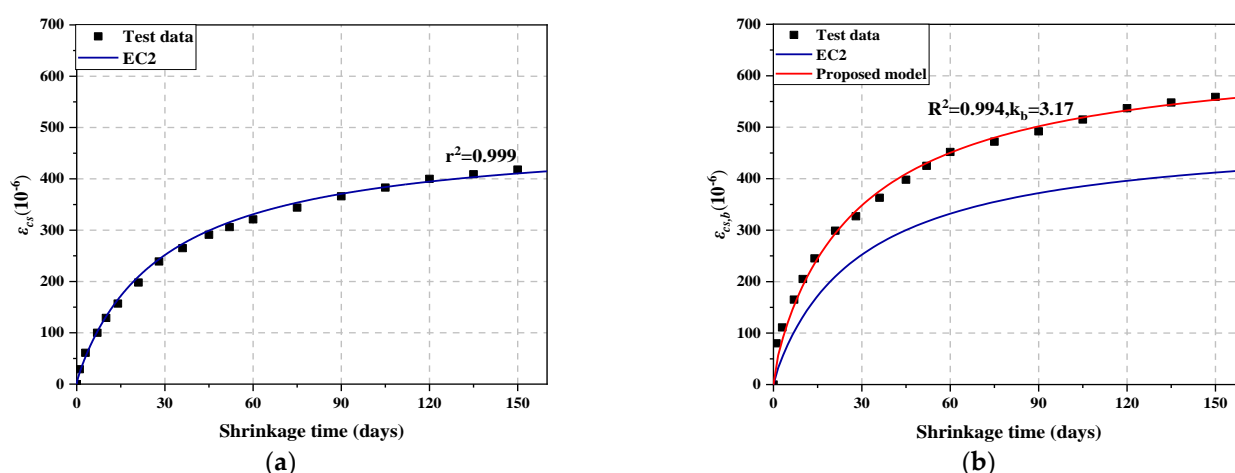


Figure 11. Predicted and tested values of (a) NAC and (b) TIC.

4.2. Time-Dependent Shrinkage Model for RATIC

Researchers found that even if RFA replaces NFA with 100% replacement ratio, the reduction of autogenous shrinkage strain ϵ_{ca} of recycled concrete is not more than 20% [17]. Therefore, the autogenous shrinkage model ($\epsilon_{ca,b}$) for TIC (Equation (6)) can be used as the

RATIC autogenous shrinkage model, and Equation (7) is the TIC drying shrinkage model ($\varepsilon_{cd,b}$). Due to the delayed effect of RFA on the development of drying shrinkage of RATIC, $\varepsilon_{cd,b}$ cannot predict the drying shrinkage strain of RATIC well. Therefore, the model of $\varepsilon_{cd,b}$ should be modified.

$$\varepsilon_{ca,b} = \left(1 - e^{-0.2t^{0.5}}\right) k_b \varepsilon_{ca}(\infty) \quad (6)$$

$$\varepsilon_{cd,b} = \frac{(t - t_0)}{(t - t_0) + 0.04\sqrt{h_0^3}} \gamma_a \varepsilon_{cd,0} \quad (7)$$

4.2.1. The Citation of Time-Dependent Factor (k_{wa})

The drying shrinkage development coefficient ($\beta(t, t_0)$) of ordinary concrete in EC2 is shown in Equation (8). In order to describe the experimental phenomenon that the drying shrinkage development time of recycled concrete is longer than that of ordinary concrete, the researchers put forward the time-dependent factor k_{wa} [21]. The modified drying shrinkage development coefficient ($\beta_a(t, t_0)$) is shown in Equations (9)–(12).

$$\beta(t, t_0) = \frac{(t - t_0)}{(t - t_0) + 0.04\sqrt{h_0^3}} \quad (8)$$

$$\beta_a(t, t_0) = \frac{(t - t_0)}{(t - t_0) + 0.04k_{wa}\sqrt{h_0^3}} \quad (9)$$

$$k_{wa} = k_{wa-F} k_{wa-C} \quad (10)$$

$$k_{wa-F} = 0.10[r_{\text{NFA}}\omega_{a-\text{RFA}} + (1 - r_{\text{RFA}})\omega_{a-\text{NFA}}] + 2.27 \quad (11)$$

$$k_{wa-C} = 0.18\omega_{a-\text{NCA}} + 0.52 \quad (12)$$

where k_{wa-C} and k_{wa-F} are the influence coefficients of shrinkage development of coarse aggregate and fine aggregate, respectively; $\omega_{a-\text{RFA}}$ is the water absorption of RFA; r_{RFA} is the replacement ratio of RFA; $\omega_{a-\text{NFA}}$ and $\omega_{a-\text{NCA}}$ are the water absorption of NFA and NCA, respectively.

In order to express the development of the drying shrinkage strain of RATIC, the difference between the predicted value of total shrinkage strain and autogenous shrinkage strain is normalized, that is, $(\varepsilon_{cs}(t) - \varepsilon_{ca,b}(t)) / (\varepsilon_{cs}(t_{\text{end}}) - \varepsilon_{ca,b}(t_{\text{end}}))$. $\beta(t, t_0)$ of the EC2 model and the modified $\beta_a(t, t_0)$ were used to fit the normalized experimental values, as shown in Figure 12a–h. It is observed that the EC2 model with the time-dependent factor k_{wa} is more helpful to describe the total shrinkage development of RATIC, so it is effective to modify the EC2 model with k_{wa} .

4.2.2. Drying Shrinkage Strain Amplification Factor k_a

According to ACI-209R-92 [41], when the quality of cement matrix is the same, the drying shrinkage deformation of ordinary concrete is mainly affected by the volume content of aggregate. The difference in the drying shrinkage between TIC and RATIC mainly lies in the type of fine aggregate. The lower elastic modulus of RFAs increase the ε_{cd} of RATIC. In order to obtain the drying shrinkage strain model of recycled concrete, researchers usually put forward the drying shrinkage amplification factor k_a based on the drying shrinkage model of ordinary concrete [42]. In summary, time-dependent shrinkage model for RATIC is shown in Equation (3).

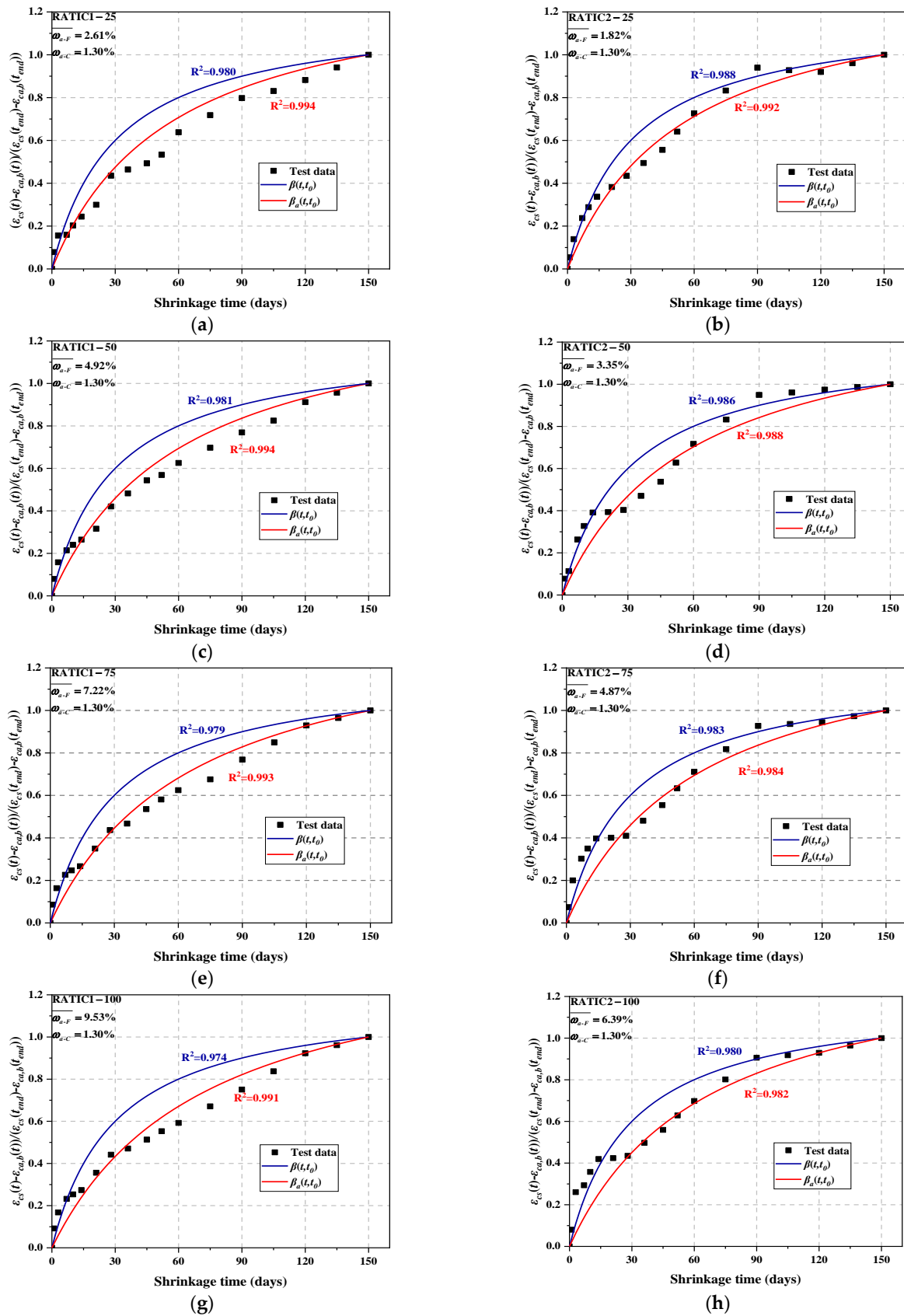


Figure 12. Comparison between the measured and calculated development of normalized total shrinkage with the time of RATIC. (a) RATIC1-25; (b) RATIC2-25; (c) RATIC1-50; (d) RATIC2-50; (e) RATIC1-75; (f) RATIC2-75; (g) RATIC1-100; (h) RATIC2-100.

Based on k_b in 4.1, γ_α and k_{wa} in 4.2.1, Figure 13 shows the RATIC amplification factor k_a obtained by regression analysis of Equation (3) based on test results, k_v is the empirical value of RFAC amplification factor obtained by Zhang et al. [21], as shown in Equation (13). Equations (14) and (15) are the fitting formula of k_a of RATIC1 and RATIC2 with the different replacement ratio of RFA, respectively.

$$k_v = \frac{1 - (V_{NA}^{RAC} + V_{RFA}^{eff})^{\frac{1}{3}}}{1 - (V_{NA}^{NAC})^{\frac{1}{3}}} \tag{13}$$

$$k_a = 1.031r_{RFA1} + 1.000 \tag{14}$$

$$k_a = 0.632r_{RFA2} + 1.000 \tag{15}$$

where V_{NA}^{RAC} and V_{NA}^{NAC} are the volume content of natural aggregate in RAC and NAC, V_{RFA}^{eff} is the effective volume content of RFA providing constraints in concrete, experience value $V_{RFA}^{eff} = 0.52V_{RFA}$ [21]. r_{RFA1} is the replacement ratio of RFA1; r_{RFA2} is the replacement ratio of RFA2.

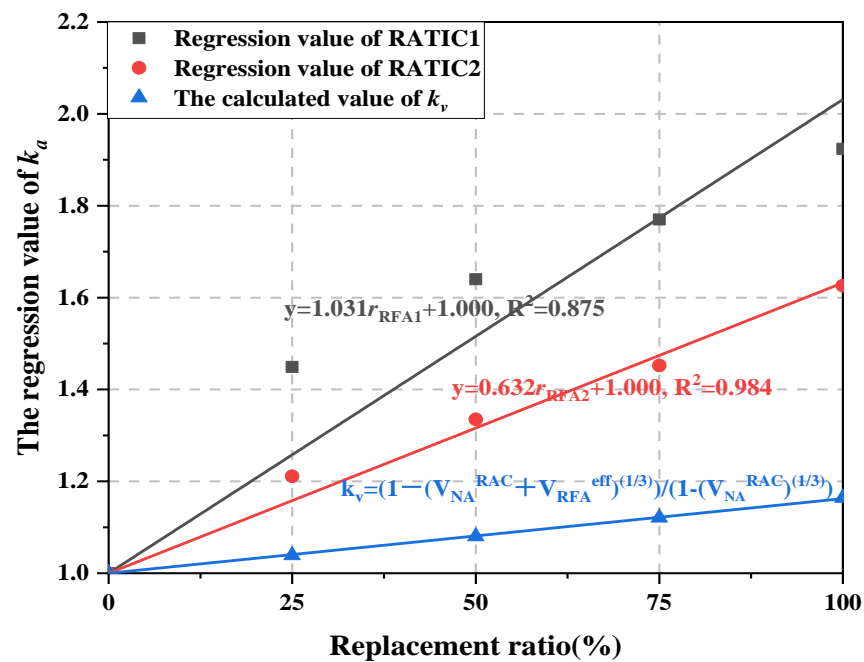


Figure 13. The regression value of k_a and empirical value k_v .

It can be seen that the regression value of k_a is greater than k_v under the same replacement ratio. This may be because the effective volume of RFA1 and RFA2 are smaller than the experience value of Zhang et al. [21]. At the same replacement ratio, k_a of RATIC1 is greater than that of RATIC2, which also indicates that the elastic modulus of RFA1 is less than that of RFA2.

4.3. Validation for the Model

In order to verify the accuracy of the model, the calculated value of k_a and k_b were substituted into Equation (13). Figure 14 shows the predicted results of EC2 model and the modified model based on the EC2 model in this study. It is not difficult to find that the EC2 model optimized by k_{wa} , k_b , k_a , and γ_α can better predict the change of the total shrinkage of RATIC. It can be observed that the time-dependent shrinkage model can predict both the development trend and final total shrinkage strain of RATIC with a maximum difference of 17%.

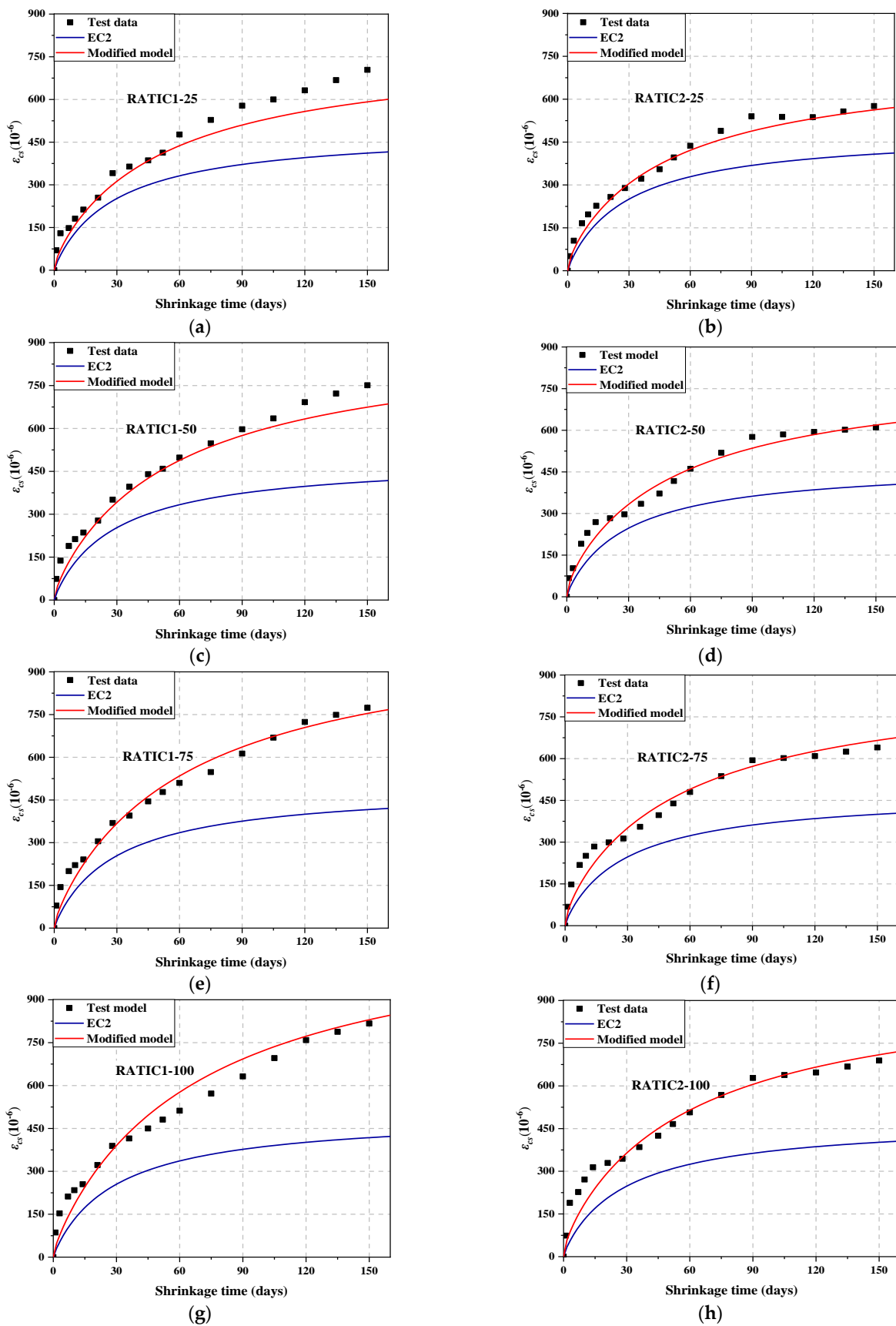


Figure 14. The predicted results of EC2 model and the modified model based on the EC2 model. (a) RATIC1-25; (b) RATIC2-25; (c) RATIC1-50; (d) RATIC2-50; (e) RATIC1-75; (f) RATIC2-75; (g) RATIC1-100; (h) RATIC2-100.

5. Conclusions

In this experiment, RATIC with GHBs was prepared by using RFA from waste concrete and waste clay brick. The shrinkage performance of RATIC was studied and a time-dependent shrinkage model for RATIC was proposed by considering the effects of GHB and RFA on RATIC shrinkage. The specific conclusions are as follows:

- Adding GHB had no obvious effect on the compressive strength of concrete before 28 days, while decreased the compressive strength after 28 days. In addition, GHB had a negative effect on the splitting tensile strength and elastic modulus of concrete at 28 days.
- The old mortar on the surface of RFA1 weakened the mechanical properties of RATIC1, and the pozzolanic reaction caused by RFA2 effectively improved the mechanical properties of RATIC2. RFA2 was more advantageous to the performance of RATIC than RFA1 in terms of chemical composition. Besides, added RFA decreased the thermal conductivity of TIC.
- The early shrinkage deformation of TIC was significantly greater than that of NAC. With the continuous development of shrinkage, the long-term shrinkage strain of TIC mixed with GHB tended to be stable. The EC2 model modified by the autogenous shrinkage amplification factor k_b can effectively predict the TIC shrinkage strain.
- The time-dependent shrinkage of RATIC was similar to that of RFAC due to the influence of water absorption of RFA, and the modified model with time-dependent factor k_{wa} can effectively predict the drying shrinkage of RATIC.
- The coefficient k_b related to GHB content and the correlation coefficient k_a related to the elastic modulus of RFA were introduced to optimize the EC2 model. The time-dependent shrinkage model for RATIC obtained can better predict the total shrinkage strain of RATIC, and the specific expression is shown as Equation (3). In future research, researchers should try to quantify the elastic modulus of different RFAs in order to predict the shrinkage strain of concrete using different RFAs.

Author Contributions: Conceptualization, X.Z., P.Z., C.C. and X.W.; methodology, X.Z., P.Z. and C.C.; software, X.Z.; validation, P.Z., C.C. and X.Y.; formal analysis, P.Z.; investigation, X.Z., P.Z. and C.C.; data curation, P.Z.; writing—original draft preparation, X.Z.; writing—review and editing, P.Z., C.C. and X.Y.; visualization, X.Z.; supervision, P.Z. and X.W.; funding acquisition, X.Z., C.C. and X.W. All authors have read and agreed to the published version of the manuscript.

Funding: This work was funded by the Prospective Joint Research Project of Jiangsu Province (No. BY2020470 and BY2020471) and the Postgraduate Research & Practice Innovation Program of Jiangsu Province (SJCX21_1191).

Institutional Review Board Statement: Not applicable.

Informed Consent Statement: Not applicable.

Data Availability Statement: The data used to support the findings of this study are available from the corresponding author upon request.

Conflicts of Interest: The authors declare no conflict of interest.

References

1. Dang, J.; Zhao, J.; Pang, S.D.; Zhao, S. Durability and microstructural properties of concrete with recycled brick as fine aggregates. *Constr. Build. Mater.* **2020**, *262*, 120032. [[CrossRef](#)]
2. Kirthika, S.K.; Singh, S.K.; Chourasia, A. Alternative fine aggregates in production of sustainable concrete—A review. *J. Clean. Prod.* **2020**, *268*, 122089. [[CrossRef](#)]
3. Wang, Y.; Zhang, H.; Geng, Y.; Wang, Q.; Zhang, S. Prediction of the elastic modulus and the splitting tensile strength of concrete incorporating both fine and coarse recycled aggregate. *Constr. Build. Mater.* **2019**, *215*, 332–346. [[CrossRef](#)]
4. Kirthika, S.K.; Singh, S.K. Durability studies on recycled fine aggregate concrete. *Constr. Build. Mater.* **2020**, *250*, 118850. [[CrossRef](#)]
5. Dang, J.; Zhao, J. Influence of waste clay bricks as fine aggregate on the mechanical and microstructural properties of concrete. *Constr. Build. Mater.* **2019**, *228*, 116757. [[CrossRef](#)]

6. Wang, W.; Liu, Y.; Qin, X.; Li, Z.; Duan, P.; Dong, X. Size effects on mechanical properties of recycled aggregate thermal insulation concrete. *Constr. Build. Mater.* **2020**, *264*, 120179. [[CrossRef](#)]
7. Zhang, Y.; Li, B.; Li, Z.; Ma, G.; Liu, Y. Seismic performance of interior beam-column joints in reinforced glazed hollow bead insulation concrete frames. *Eng. Struct.* **2021**, *228*, 111494. [[CrossRef](#)]
8. Guo, Y.; Liu, Y.; Wang, W.; Zhang, Y.; Wang, Z.; Jiang, L. A study on heat transfer performance of recycled aggregate thermal insulation concrete. *J. Build. Eng.* **2020**, *32*, 101797. [[CrossRef](#)]
9. Wang, W.; Zhao, L.; Liu, Y.; Li, Z. Mechanical properties and stress–strain relationship in axial compression for concrete with added glazed hollow beads and construction waste. *Constr. Build. Mater.* **2014**, *71*, 425–434. [[CrossRef](#)]
10. Xiao, J.; Song, Z.; Zhang, F. Test and analysis of thermal conductivity of concrete. *J. Build. Mater.* **2010**, *13*, 17–21.
11. Zhao, L.; Wang, W.; Li, Z.; Chen, Y.F. An experimental study to evaluate the effects of adding glazed hollow beads on the mechanical properties and thermal conductivity of concrete. *Mater. Res. Innov.* **2015**, *19*, 929–935. [[CrossRef](#)]
12. Lahmar, N.; Bouziadi, F.; Boulekbache, B.; Meziane, E.-H.; Hamrat, M.; Haddi, A.; Djelal, C. Experimental and finite element analysis of shrinkage of concrete made with recycled coarse aggregates subjected to thermal loading. *Constr. Build. Mater.* **2020**, *247*, 118564. [[CrossRef](#)]
13. Wang, Q.; Ranzi, G.; Wang, Y.; Geng, Y. Long-term behaviour of simply-supported steel-bars truss slabs with recycled coarse aggregate. *Constr. Build. Mater.* **2016**, *116*, 335–346. [[CrossRef](#)]
14. European Committee of Standardization. *Eurocode 2: Design of Concrete Structures-Part 1–1: General Rules and Rules for Buildings*; European Committee of Standardization: Brussels, Belgium, 2004.
15. Holt, E. Contribution of mixture design to chemical and autogenous shrinkage of concrete at early ages. *Cem. Concr. Res.* **2005**, *35*, 464–472. [[CrossRef](#)]
16. Delsaute, B.; Staquet, S. Development of Strain-Induced Stresses in Early Age Concrete Composed of Recycled Gravel or Sand. *J. Adv. Concr. Technol.* **2019**, *17*, 319–334. [[CrossRef](#)]
17. Zhang, H.; Wang, Y.-Y.; Lehman, D.E.; Geng, Y. Autogenous-shrinkage model for concrete with coarse and fine recycled aggregate. *Cem. Concr. Compos.* **2020**, *111*, 103600. [[CrossRef](#)]
18. Zhang, H.; Yuan, H.; Ge, Z.; Wu, J.; Fang, C.; Schlangen, E.; Šavija, B. Fresh and hardened properties of self-compacting concrete containing recycled fine clay brick aggregates. *Mater. Struct.* **2021**, *54*, 1–13. [[CrossRef](#)]
19. Seo, T.; Lee, M.; Choi, C.; Ohno, Y. Properties of drying shrinkage cracking of concrete containing fly ash as partial replacement of fine aggregate. *Mag. Concr. Res.* **2010**, *62*, 427–433. [[CrossRef](#)]
20. Khatib, J.M. Properties of concrete incorporating fine recycled aggregate. *Cem. Concr. Res.* **2005**, *35*, 763–769. [[CrossRef](#)]
21. Zhang, H.; Wang, Y.; Lehman, D.E.; Geng, Y.; Kuder, K. Time-dependent drying shrinkage model for concrete with coarse and fine recycled aggregate. *Cem. Concr. Compos.* **2020**, *105*, 103426. [[CrossRef](#)]
22. Maghfouri, M.; Shafiqh, P.; Alimohammadi, V.; Doroudi, Y.; Aslam, M. Appropriate drying shrinkage prediction models for lightweight concrete containing coarse agro-waste aggregate. *J. Build. Eng.* **2020**, *29*, 101148. [[CrossRef](#)]
23. Mao, Y.; Liu, J.; Shi, C. Autogenous shrinkage and drying shrinkage of recycled aggregate concrete: A review. *J. Clean. Prod.* **2021**, *295*, 126435. [[CrossRef](#)]
24. Van Bunderen, C.; Benboudjema, F.; Snellings, R.; Vandewalle, L.; Cizer, Ö. Experimental analysis and modelling of mechanical properties and shrinkage of concrete recycling flash calcined dredging sediments. *Cem. Concr. Compos.* **2021**, *115*, 103787. [[CrossRef](#)]
25. Lai, M.H.; Binhowimal, S.A.M.; Griffith, A.M.; Hanzic, L.; Wang, Q.; Chen, Z.; Ho, J.C.M. Shrinkage design model of concrete incorporating wet packing density. *Constr. Build. Mater.* **2021**, *280*, 122448. [[CrossRef](#)]
26. Standardization Administration of China. *GB 175-2007-Common Portland Cement*; Standardization Administration of China: Beijing, China, 2007.
27. Zhu, P.; Xu, X.; Liu, H.; Liu, S.; Chen, C.; Jia, Z. Tunnel fire resistance of self-compacting concrete coated with SiO₂ aerogel cement paste under 2.5 h HC fire loading. *Constr. Build. Mater.* **2020**, *239*, 117857. [[CrossRef](#)]
28. Standardization Administration of China. *GB/T 14684-2011-Sand for Construction*; Standardization Administration of China: Beijing, China, 2011.
29. Standardization Administration of China. *GB/T 14685-2011-Pebble and Crushed Stone for Construction*; Standardization Administration of China: Beijing, China, 2011.
30. Castro, J.; Keiser, L.; Goliass, M.; Weiss, W. Absorption and desorption properties of fine lightweight aggregate for application to internally cured concrete mixtures. *Cem. Concr. Compos.* **2011**, *33*, 1001–1008. [[CrossRef](#)]
31. Li, Z.; Liu, J.; Xiao, J.; Zhong, P. A method to determine water absorption of recycled fine aggregate in paste for design and quality control of fresh mortar. *Constr. Build. Mater.* **2019**, *197*, 30–41. [[CrossRef](#)]
32. ASTM. *ASTM C618-Standard Specification for Coal Fly Ash and Raw or Calcined Natural Pozzolan for Use in Concrete*; ASTM International: West Conshohocken, PA, USA, 2019.
33. He, Z.; Shen, A.; Wu, H.; Wang, W.; Wang, L.; Yao, C.; Wu, J. Research progress on recycled clay brick waste as an alternative to cement for sustainable construction materials. *Constr. Build. Mater.* **2021**, *274*, 122113. [[CrossRef](#)]
34. Geng, Y.; Zhao, M.; Yang, H.; Wang, Y. Creep model of concrete with recycled coarse and fine aggregates that accounts for creep development trend difference between recycled and natural aggregate concrete. *Cem. Concr. Compos.* **2019**, *103*, 303–317. [[CrossRef](#)]

35. Cartuxo, F.; de Brito, J.; Evangelista, L.; Jiménez, J.R.; Ledesma, E.F. Rheological behaviour of concrete made with fine recycled concrete aggregates—Influence of the superplasticizer. *Constr. Build. Mater.* **2015**, *89*, 36–47. [[CrossRef](#)]
36. Ministry of Housing and Urban-Rural Development of the People's Republic of China. *GB/T 50080-2016-Standard Test Method for Performance of Ordinary Concrete Mixtures*; Ministry of Housing and Urban-Rural Development of the People's Republic of China: Beijing, China, 2016.
37. Ministry of Housing and Urban-Rural Development of the People's Republic of China. *GB/T50081-2019-Standard for Test Methods of Physical and Mechanical Properties of Concrete*; Ministry of Housing and Urban-Rural Development of the People's Republic of China: Beijing, China, 2019.
38. Ministry of Housing and Urban-Rural Development of the People's Republic of China. *GB/T 50082-2009-Standard for Test Methods of Long-term Performance and Durability of Ordinary Concrete*; Ministry of Housing and Urban-Rural Development of the People's Republic of China: Beijing, China, 2009.
39. Hao, L.; Liu, Y.; Xiao, J. Durability of recycled aggregate thermal insulation concrete under combined flexural loading and freeze–thaw cycles. *Constr. Build. Mater.* **2021**, *272*, 121652. [[CrossRef](#)]
40. Lu, T.; Li, Z.; Huang, H. Restraining effect of aggregates on autogenous shrinkage in cement mortar and concrete. *Constr. Build. Mater.* **2021**, *289*, 123166. [[CrossRef](#)]
41. ACI. *ACI 209R-92-Prediction of Creep, Shrinkage, and Temperature Effects in Concrete Structures*; ASTM International: West Conshohocken, PA, USA, 1992.
42. De Brito, J.; Alves, F. Concrete with recycled aggregates: The Portuguese experimental research. *Mater. Struct.* **2010**, *43*, 35–51. [[CrossRef](#)]